frontiers

Supplementary Material for "Drivers of Marine Heatwaves: A Global Analysis With an Earth System Model"

Temperature tendency term budget in GFDL ESM2M

The total heat flux (in $\mathrm{W\,m^{-2}}$) over a time step at a given grid cell in MOM4p1 is given by (Griffies, 2015)

$$\Delta Q_{\text{tot}} = \Delta Q_{\text{a-s}} + \Delta Q_{\text{vmix}} + \Delta Q_{\text{vdiff}} + \Delta Q_{\text{adv}} + \Delta Q_{\text{res}}, \tag{S1}$$

where

$$\Delta Q_{\text{a-s}} = \Delta Q_{\text{temp\_vdiffuse\_sbc}} + \Delta Q_{\text{sw\_heat}} \tag{S2}$$

$$\Delta Q_{\text{vmix}} = \Delta Q_{\text{temp\_nonlocal\_kpp}} \tag{S3}$$

$$\Delta Q_{\text{vdiff}} = \Delta Q_{\text{temp\_vdiffuse\_impl}} - \Delta Q_{\text{temp\_vdiffuse\_sbc}} \tag{S4}$$

$$\Delta Q_{\text{adv}} = \Delta Q_{\text{temp\_advection}} + \Delta Q_{\text{neutral\_gm\_temp}} + \Delta Q_{\text{temp\_submeso}} \tag{S5}$$

$$\begin{aligned}\Delta Q_{\text{res}} = {} & \Delta Q_{\text{sfc\_hflux\_pme}} + \Delta Q_{\text{neutral\_diffusion\_temp}} + \Delta Q_{\text{temp\_sigma\_diff}} \\ & + \Delta Q_{\text{mixdownslope\_temp}} + \Delta Q_{\text{temp\_runoffmix}} + \Delta Q_{\text{temp\_calvingmix}} \\ & + \Delta Q_{\text{temp\_xland}} + \Delta Q_{\text{temp\_xlandinsert}} + \Delta Q_{\text{frazil\_2d}} \\ & + \Delta Q_{\text{temp\_eta\_smooth}}.\end{aligned} \tag{S6}$$

Table S1. A detailed description of the temperature tendency terms implemented in MOM4p1. Further information on each term is given in Griffies (2009) and Griffies (2012).

Term	Short description
$\Delta Q_{\text{temp\_vdiffuse\_sbc}}$	Sum of shortwave, longwave, latent and sensible heat fluxes at the ocean surface
$\Delta Q_{\text{sw\_heat}}$	Penetrative shortwave radiation below surface
$\Delta Q_{\text{temp\_nonlocal\_kpp}}$	Convective vertical mixing from the nonlocal part of the K-Profile Parametrization (KPP)
$\Delta Q_{\text{temp\_vdiffuse\_impl}}$	Sum of the temp_vdiffuse_sbc term and heat flux from vertical diffusion from the local part of the KPP scheme, as well as tidal mixing and geothermal heating
$\Delta Q_{\text{temp\_advection}}$	Resolved advection
$\Delta Q_{\text{neutral\_gm\_temp}}$	Parametrized mesoscale advection
$\Delta Q_{\text{temp\_submeso}}$	Parametrized submesoscale advection
$\Delta Q_{\text{sfc\_hflux\_pme}}$	Heat flux from heat content of water exchanged across the surface through precipitation and evaporation
$\Delta Q_{\text{neutral\_diffusion\_temp}}$	Parametrized neutral diffusion
$\Delta Q_{\text{temp\_sigma\_diff}}$	Diffusion in turbulent layer along bottom topography
$\Delta Q_{\text{mixdownslope\_temp}}$	Deep water formation near steep topography
$\Delta Q_{\text{temp\_runoffmix}}$	Liquid runoff (rivers) from the land model
$\Delta Q_{\text{temp\_calvingmix}}$	Solid runoff (iceberg calving) from the land model
$\Delta Q_{\text{temp\_xland}}$	Exchange between marginal seas and open ocean across unresolved narrow passages through constant mixing
$\Delta Q_{\text{temp\_xlandinsert}}$	Exchange between marginal seas and open ocean across unresolved narrow passages through insertion of water volumes proportional to cross-land sea surface height difference
$\Delta Q_{\text{frazil\_2d}}$	Formation of frazil ice
$\Delta Q_{\text{temp\_eta\_smooth}}$	Handling of a model grid artifact

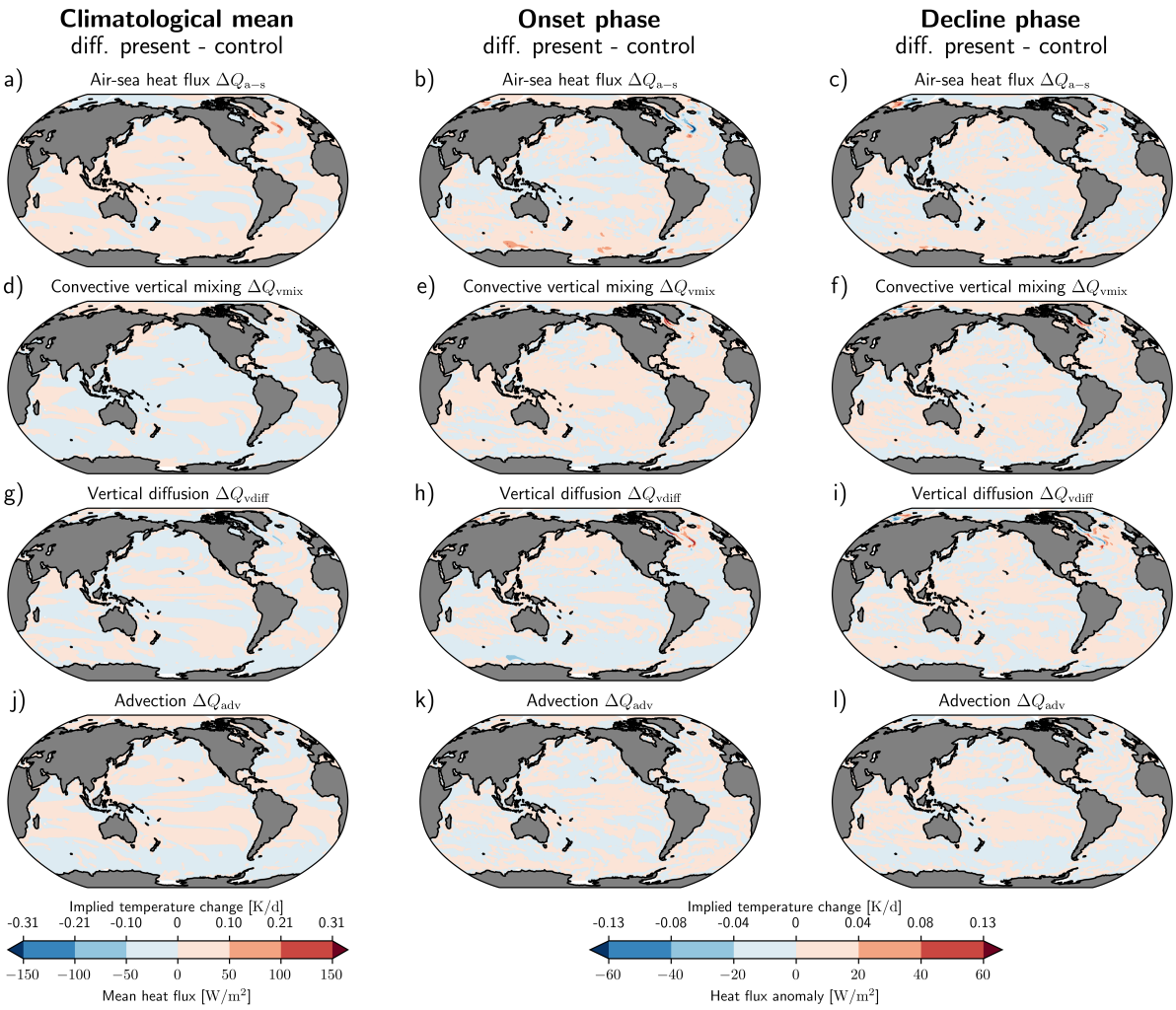

Figure S1. Difference of the local drivers between the preindustrial simulation as used in the main text and the mean of an eight-member ensemble simulation using historical and RCP8.5 forcing for the present period 1982–2021. The four most important heat and temperature tendency terms are shown (left column; a, d, g, j) for the climatological mean, (center column; b, e, h, k) during the onset phase of marine heatwaves, and (right column; c, f, i, l) during the decline phase of marine heatwaves. The patterns during the onset and decline phase were obtained by averaging daily surface tendency term anomalies of each term over all onset and decline days of MHWs, respectively. Implied temperature changes (units in $\mathrm{K\,d^{-1}}$) were computed assuming a constant grid cell thickness.

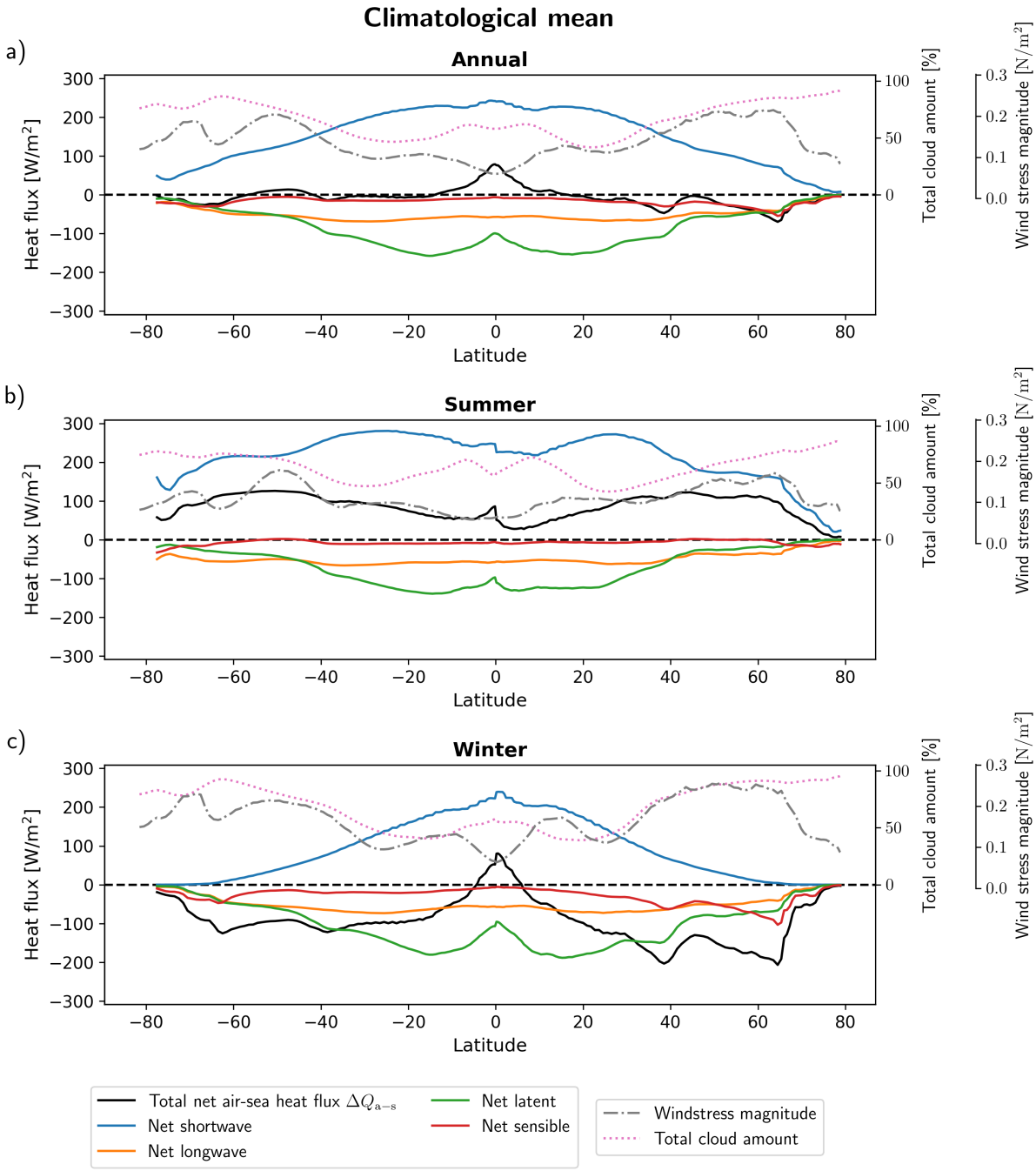

Figure S2. Individual contributions to the zonal mean total net air-sea heat flux for the (a) climatological mean (averaged over the whole year), for summer (averaged over JJA for Northern Hemisphere and DJF for Southern Hemisphere), and for winter (averaged over DJF for Northern Hemisphere and JJA for Southern Hemisphere) averaged over the 500-yr preindustrial control simulation. The individual contributions are net shortwave and net longwave radiation, as well as net latent and sensible heat fluxes. Wind stress magnitude and total cloud amount are also shown.

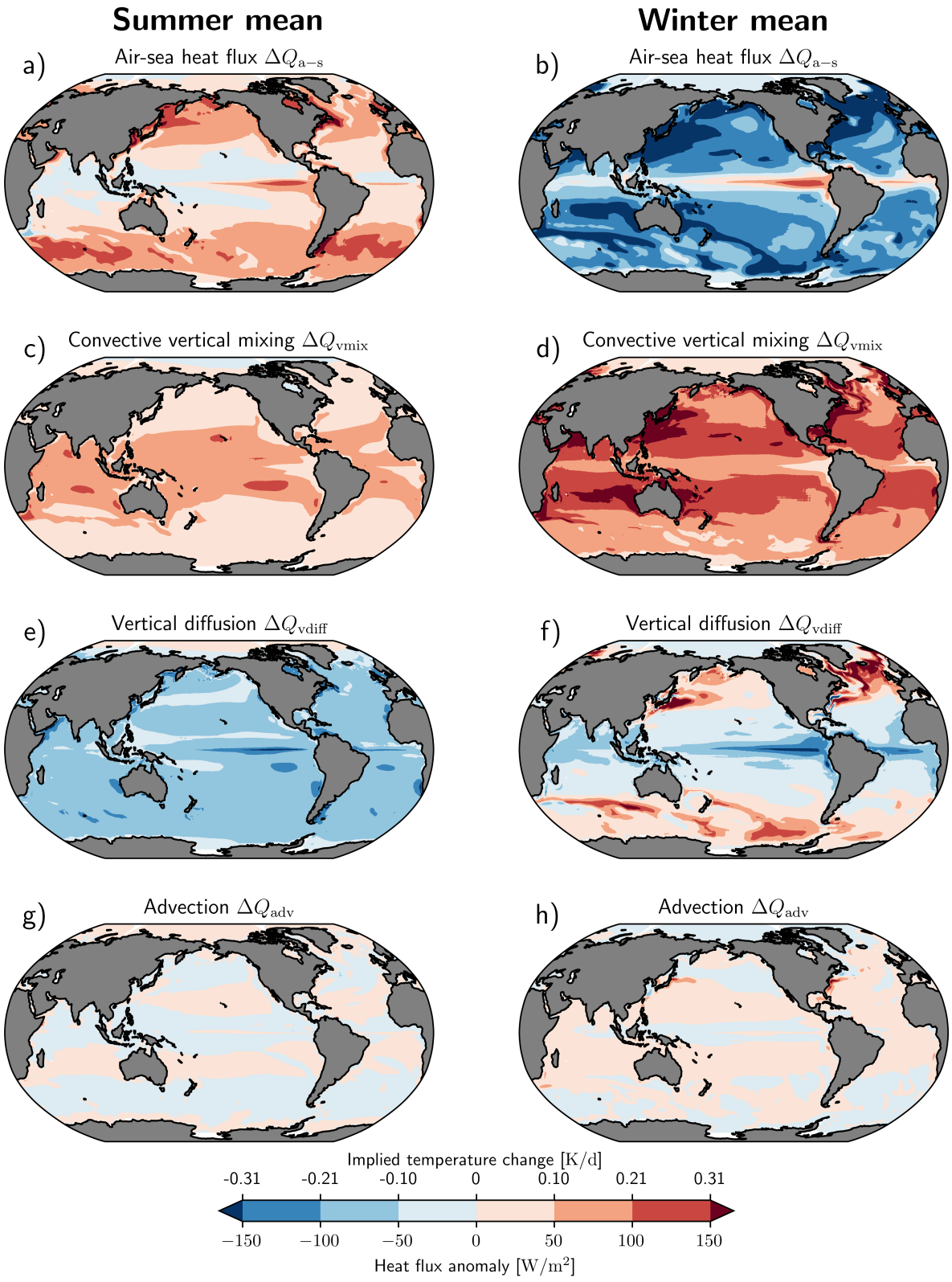

Figure S3. Seasonal decomposition of MHW driver anomaly patterns in the climatological mean averaged over the 500-yr preindustrial control simulation. Heat fluxes from the four most important MHW drivers averaged in time during summer (first column; a, c, e, g) and winter (second column; b, d, f, h) are shown. For summer, the average over JJA in the Northern Hemisphere and DJF in the Southern Hemisphere is shown simultaneously. For winter, the average over DJF in the Northern Hemisphere and JJA for the Southern Hemisphere is shown simultaneously.

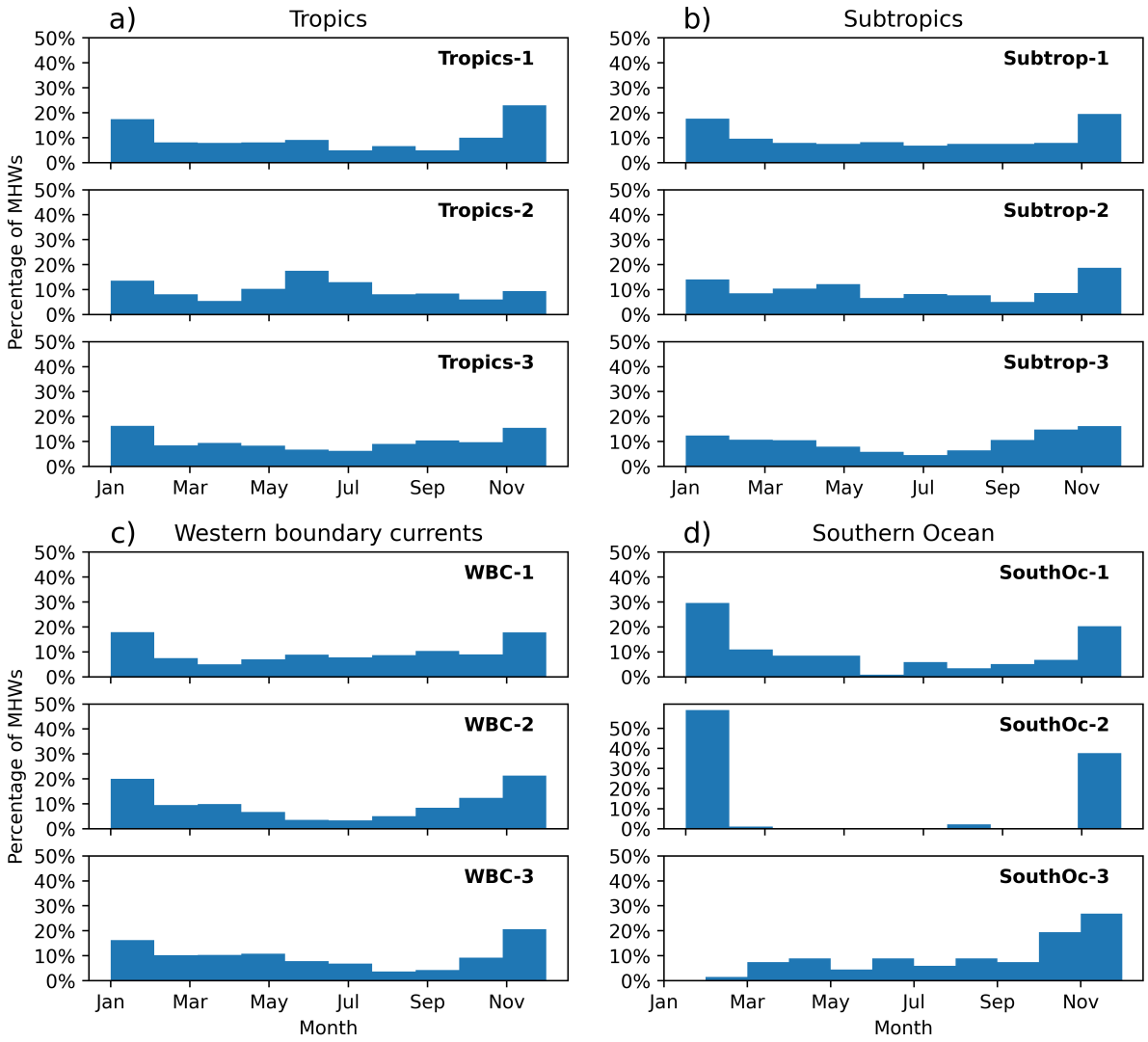

Figure S4. Month of peak SST anomaly for MHW types in four selected regions: a) Tropics, b) Subtropics, c) Western boundary currents, and d) Southern Ocean. The histogram bars indicate the distribution of each region's MHWs over the months of the year. The regions are shown in Figure 8 of the main text. Regional MHWs are defined by averaging SST over these latitude-longitude boxes and applying the MHW definition (section 2.2 of the main text) to the resulting time series.

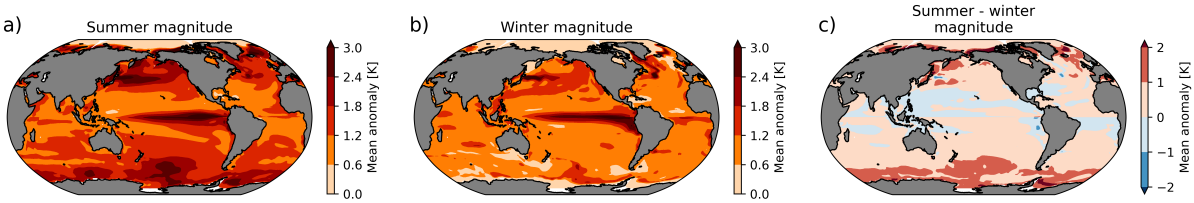

Figure S5. Seasonal patterns of simulated sea surface temperature anomaly relative to the seasonal cycle averaged over marine heatwave days in the 500-yr preindustrial ESM2M simulation; for (a) summer, (b) winter, and (c) the difference between summer and winter.

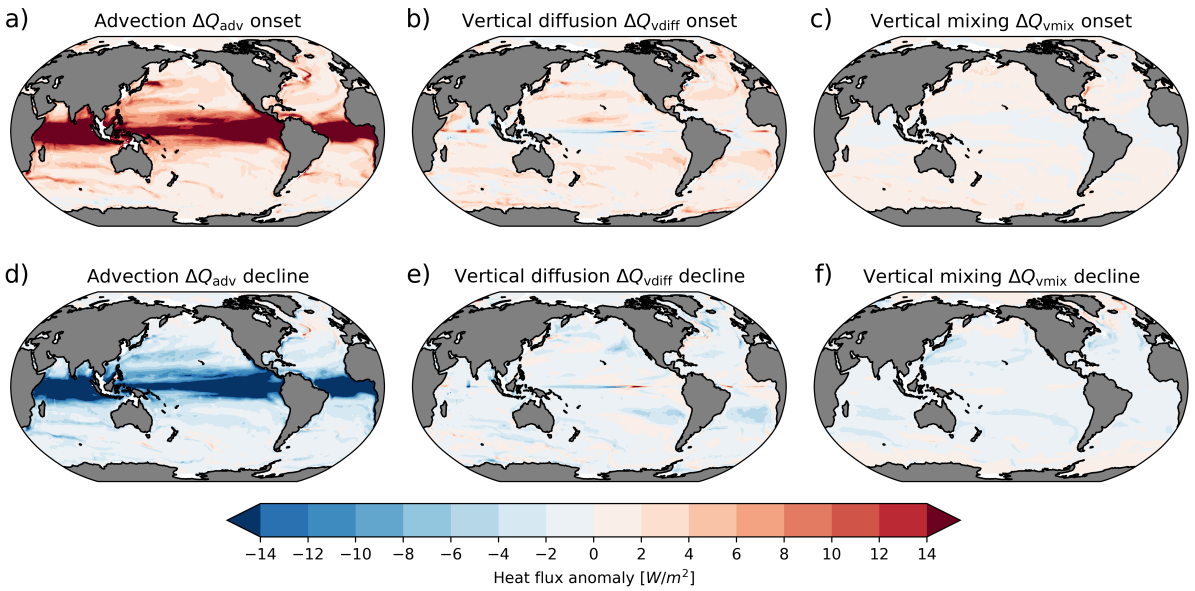

Figure S6. Simulated patterns of the three most important local drivers of MHWs at 95 meters depth during the onset phase (a, b, c), and during the decline phase of MHWs (d, e, f). The patterns during the onset and decline phase were obtained by averaging daily tendency term anomalies of each term over all onset and decline days of MHWs at 95 meters depth, respectively.

REFERENCES

Griffies, S. M. (2009). Elements of MOM4p1. https://mom-ocean.github.io/assets/pdfs/MOM4p1_manual.pdf [Accessed December 1, 2021].

Griffies, S. M. (2012). Elements of the Modular Ocean Model (MOM). https://mom-ocean.github.io/assets/pdfs/MOM5_manual.pdf [Accessed December 1, 2021].

Griffies, S. M. (2015). Working notes on the ocean heat budget in GFDL-ESM2M. https://mom-ocean.github.io/assets/pdfs/ESM2M_heat_budget.pdf [Accessed December 1, 2021].